

A SPATIAL-DOMAIN METHOD OF MOMENTS ANALYSIS OF A CYLINDRICAL-RECTANGULAR CHIROSTRIP

L.-W. Li [†]

Department of Electrical and Computer Engineering
National University of Singapore
10 Kent Ridge Crescent, Singapore 119260

T.-X. Zhao

Department of Electrical and Computer Engineering
University of Houston
Houston, TX 77204-4793, USA

M.-S. Leong and T.-S. Yeo

Department of Electrical and Computer Engineering
National University of Singapore
10 Kent Ridge Crescent, Singapore 119260

Abstract—In this paper, a spatial-domain Galerkin's procedure in Method of Moments is applied to analyse a cylindrical-rectangular chirostrip antenna. It is assumed that a single-layer chiral substrate is wrap-fabricated around a conducting core-cylinder and that a perfectly conducting and electrically thin rectangular-cylindrical microstrip patch antenna is mounted on the surface of the chiral substrate. By imposing the boundary conditions on the multiple interfaces and applying the scattering superposition method, a complete expression of dyadic Green's functions (DGFs) has been obtained and the current distribution over the cylindrical rectangular chirostrip antenna has been determined. Various radiation patterns due to such a microstrip antenna in the presence of a chiral substrate are obtained and compared with those in the presence of an achiral substrate, so as to gain physical insight into effects of the chirostrip.

[†] High-Performance Computations for Engineered Systems Programme, Singapore-MIT Alliance (SMA), 10 Kent Ridge Crescent, Singapore 119260

1 Introduction

2 Formulation of the Problem

- 2.1 The Chiral Substrate
- 2.2 Dyadic Green's Functions
- 2.3 Galerkin's Method of Moments Procedure
 - 2.3.1 Currents on the Feed Line
 - 2.3.2 Microstrip Patch Currents
 - 2.3.3 Junction Overlap Currents
- 2.4 Far-Field Radiation Patterns

3 Numerical Results and Discussion

4 Conclusions

References

1. INTRODUCTION

The analysis of printed microstrip antenna has attracted considerable interests of many scientists and engineers in the last several decades, due to its low cost, good reliability, and wide applications. Cylindrical-rectangular microstrip antennas have also found many potential applications because they can be flush-mounted on curved (such as conical) surfaces. Krowné [1] calculated the resonant frequencies while Wu and Kaufman [2] computed the radiation patterns. Wong and Chen [3] and Ke and Wong [4] calculated the resonant frequency of a slot-coupled cylindrical rectangular microstrip antenna and input impedance of a probe-fed superstrate-loaded cylindrical rectangular microstrip antenna. Wong *et al.* [5] also analysed the resonance problem of the cylindrical rectangular microstrip structure with an airgap between the substrate layer and the ground cylinder. Mutual coupling [6], superstrate loading effects [7], and broadband effects of antennas designed using gap-coupled parasitic patches [4] were also reported.

The dyadic Green's function (DGF) technique has been widely used to characterise electromagnetic waves [8–12] for more than two decades. The DGFs in multilayered structures are of particular interest to many engineers and scientists because of their good accuracy, compact form, and flexibility of current distribution expressions in modeling practical problems. The DGF technique is also a powerful tool for solving various boundary-value problems of electromagnetic chiralities. Some research works have been carried out in formulating

the DGFs in unbounded chiral media, planar-stratified chiral media, spherically multilayered chiral media, and cylindrically multilayered chiral media. The formulation of dyadic Green's functions for the cylindrical multilayered chiral media, which can be used to analyze the radiation properties of electric and magnetic sources (such as chirostrip antenna) embedded in multilayered chiral media has been recently documented [13, 14]. However, the DGF for the present structure under consideration in this paper is not available yet.

Earlier in 1991 [15, 16], a new type of microstrip using chiral material was introduced and its characteristics have been discussed. For instance, effects of chirality on the surface-wave power excited by a two-dimensional chirostrip antenna have been studied by Pelet and Engheta [17]. Toscano and Vegni have analyzed the radiated characteristics of an electric point source located vertically at the interface-plane of a grounded chiral slab using the spectral dyadic Green's function formulation [18]. Kluskens and Newman [19] have also presented a spectral-domain Galerkin's procedure in the moment method solution for a microstrip transmission line on a chiral substrate. In 1993, Yin and Wang [20] investigated effects of a chiral superstrate on radiation characteristics of a horizontal dipole antenna printed on a grounded chiral slab. Zhao *et al.* [21] have recently investigated the radiation characteristics of a rectangular chirostrip antenna, and derived the spectral-domain dyadic Green's function expression for such an antenna structure using the Spectral-Domain Immittance Approach.

From previous works, it is seen that previous analyses assumed simple antennas, *e.g.*, an infinitesimal dipole and a transmission line antenna. A more practical configuration of this kind of problems is planar and cylindrical multilayered geometries where one (or more) of the multiple regions is (or are) filled with chiral materials. To date, nothing has been reported, to the best of the authors' knowledge, on the cylindrical-rectangular chirostrip antenna radiation.

In the paper, a cylindrical-rectangular chirostrip antenna fed by a microstrip line mounted on a circular cylindrical chiral substrate with a conducting core-cylinder is analysed. The spatial-domain Galerkin's procedure in method of moments is employed in the present analysis. To solve the problem for the solution, the dyadic Green's functions of the electric type in a concentric cylindrical chiral-medium geometry of three layers (where the outer region is air, the inner region is a conducting core-cylinder, and the intermediate layer is the chiral-material-coated substrate) are obtained. In addition, the current distribution over the microstrip antenna is then determined. The numerical results are obtained and plotted to show effects of chirality

admittance of the chiral substrate. Various radiation patterns of the microstrip antenna in the presence of a chiral substrate are obtained and compared among themselves and with those in the presence of an isotropic substrate.

2. FORMULATION OF THE PROBLEM

The microstrip cylindrical structure is shown in Figure 1(a). A very thin and perfectly conducting patch is printed on a cylindrical dielectric chiral substrate of thickness $h = b - a$. The patch is a cylindrical-rectangular element with dimensions of $2d_0 \times w_0$ at $\rho = b$. The substrate is coated on a perfectly conducting ground cylinder of radius $\rho = a$. The outer medium is assumed to be filled with air and has a free-space permittivity of ϵ_0 . Both the ground cylinder and the coated cylindrical substrate layer are assumed to be infinite along \hat{z} -direction.

2.1. The Chiral Substrate

Throughout the paper, a time-dependence of $e^{-i\omega t}$ is assumed and suppressed. Thus, homogeneous, lossless, chiral materials are characterised by the following constitutive relationships

$$\mathbf{D} = \epsilon_c \mathbf{E} + i\xi_c \mathbf{H}, \quad (1a)$$

$$\mathbf{B} = \mu \mathbf{H} - i\xi_c \mathbf{E}, \quad (1b)$$

where ϵ_c is the permittivity of the medium, μ denotes its permeability, and ξ_c stands for its chiral admittance, respectively. The chiral parameter, ξ_c , is a measure of chirality of the medium. The eigenmodes of propagation in such a medium are those of right- and left-handed circularly polarized (RCP and LCP) waves of wavenumbers given by

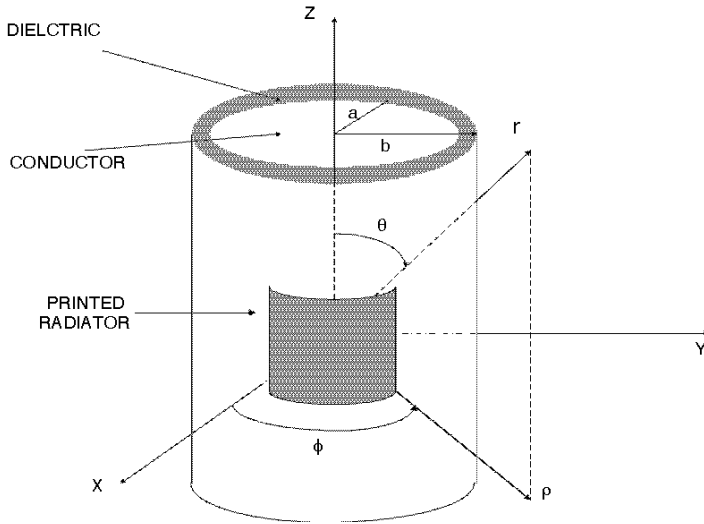
$$k^{(r)} = +\omega\mu_c\xi_c + \sqrt{\omega^2\mu_c\epsilon_c + (\omega\mu_c\xi_c)^2}, \quad (2a)$$

$$k^{(l)} = -\omega\mu_c\xi_c + \sqrt{\omega^2\mu_c\epsilon_c + (\omega\mu_c\xi_c)^2} \quad (2b)$$

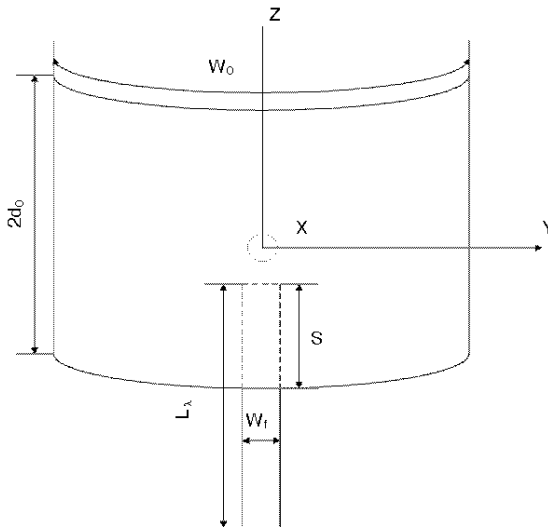
where the plus ('+') sign corresponds to RCP waves ($k^{(r)}$) while the minus sign ('-') to LCP waves ($k^{(l)}$).

2.2. Dyadic Green's Functions

Making use of the method of scattering superposition, we may decompose the dyadic Green's function $\overline{\mathbf{G}}_e^{(fs)}(\mathbf{r}, \mathbf{r}')$ into two parts, *i.e.*,



(a) Geometry of the radiating system.



(b) A cylindrical-rectangular microstrip antenna and its microstrip line feeding element.

Figure 1. Geometry of a rectangular-cylindrical microstrip antenna printed on a chiral substrate coated on the surface of a metallic core-cylinder.

the unbounded dyadic Green's function $\overline{\mathbf{G}}_{e0}(\mathbf{r}, \mathbf{r}')$ and the scattering dyadic Green's function $\overline{\mathbf{G}}_{es}^{(fs)}(\mathbf{r}, \mathbf{r}')$, as follows:

$$\overline{\mathbf{G}}_e^{(fs)}(\mathbf{r}, \mathbf{r}') = \overline{\mathbf{G}}_{e0}(\mathbf{r}, \mathbf{r}')\delta_f^s + \overline{\mathbf{G}}_{es}^{(fs)}(\mathbf{r}, \mathbf{r}') \quad (3)$$

where δ_f^s ($= 0$ if $f \neq s$ and 1 if $f = s$) stands for the Kronecker delta, the superscript (fs) denotes the layers where the *field* point and the *source* point are located, respectively, while the subscript s identifies the *scattering* dyadic Green's function and the subscript e stands for the *electric* type of dyadic Green's function. Also, the prime denotes the cylindrical coordinates (r', ϕ', z') of the current source \mathbf{J}_s . The unbounded dyadic Green's function, $\mathbf{G}_{e0}(\mathbf{r}, \mathbf{r}')$, represents the contribution of the direct waves from radiation sources in a unbounded medium, and the scattering dyadic Green's function, $\mathbf{G}_{es}^{(fs)}(\mathbf{r}, \mathbf{r}')$, describes an additional contribution of the multiply reflected and transmitted waves due to the cylindrical interfaces of the layered media.

The unbounded dyadic Green's function for the chiral medium, consisting of an irrotational term and a principal value, can be represented in terms of the normalized cylindrical vector wave functions. Using the method for deriving the dyadic Green's function by Tai [8], the unbounded dyadic Green's function under the cylindrical coordinate system can be expressed [13, 14] for $r \gtrsim r'$ as follows:

$$\overline{\mathbf{G}}_{e0}(\mathbf{r}, \mathbf{r}') = -\frac{\widehat{\mathbf{z}}\widehat{\mathbf{z}}\delta(\mathbf{r} - \mathbf{r}')}{k_s^2} + \frac{i}{4\pi(k_s^{(r)} + k_s^{(l)})} \int_{-\infty}^{\infty} dh \sum_{n=0}^{\infty} (2 - \delta_n^0) \times \left\{ \begin{array}{l} \frac{k_s^{(r)}}{[\eta_s^{(r)}]^2} \mathbf{V}_{e_{0n\eta_s^{(r)}}}^{(1)}(h) \mathbf{V}'_{e_{0n\eta_s^{(r)}}}(-h) \\ \quad + \frac{k_s^{(l)}}{[\eta_s^{(l)}]^2} \mathbf{W}_{e_{0n\eta_s^{(l)}}}^{(1)}(h) \mathbf{W}'_{e_{0n\eta_s^{(l)}}}(-h), \\ \frac{k_s^{(r)}}{[\eta_s^{(r)}]^2} \mathbf{V}_{e_{0n\eta_s^{(r)}}}(h) \mathbf{V}'_{e_{0n\eta_s^{(r)}}}(1)(-h) \\ \quad + \frac{k_s^{(l)}}{[\eta_s^{(l)}]^2} \mathbf{W}_{e_{0n\eta_s^{(l)}}}(h) \mathbf{W}'_{e_{0n\eta_s^{(l)}}}(1)(-h); \end{array} \right. \quad (4)$$

where the modified cylindrical vector wave eigenfunctions, \mathbf{V} and \mathbf{W} ,

are given in [13]:

$$\begin{aligned}
 \mathbf{V}_{e_{on\eta_s^{(r)}}}(h) &= \frac{1}{\sqrt{2}} \left[\mathbf{M}_{e_{on\eta_s^{(r)}}}(h) + \mathbf{N}_{e_{on\eta_s^{(r)}}}(h) \right] \\
 &= \frac{e^{ihz}}{\sqrt{2}} \left\{ \mp \frac{nJ_n(\eta_s^{(r)}r)}{r} \cdot \frac{\sin(n\phi)}{\cos(n\phi)} \left(\hat{\mathbf{r}} + \frac{ih}{k_s^{(r)}} \hat{\boldsymbol{\phi}} \right) \right. \\
 &\quad \left. + \frac{\partial J_n(\eta_s^{(r)}r)}{\partial r} \cdot \frac{\cos(n\phi)}{\sin(n\phi)} \left(\frac{ih}{k_s^{(r)}} \hat{\mathbf{r}} - \hat{\boldsymbol{\phi}} \right) \right. \\
 &\quad \left. + \frac{(\eta_s^{(r)})^2}{k_s^{(r)}} J_n(\eta_s^{(r)}r) \frac{\cos(n\phi)}{\sin(n\phi)} \hat{\mathbf{z}} \right\}, \quad (5a)
 \end{aligned}$$

$$\begin{aligned}
 \mathbf{W}_{e_{on\eta_s^{(l)}}}(h) &= \frac{1}{\sqrt{2}} \left[\mathbf{M}_{e_{on\eta_s^{(l)}}}(h) - \mathbf{N}_{e_{on\eta_s^{(l)}}}(h) \right] \\
 &= \frac{e^{ihz}}{\sqrt{2}} \left\{ \pm \frac{nJ_n(\eta_s^{(l)}r)}{r} \cdot \frac{\sin(n\phi)}{\cos(n\phi)} \left(\hat{\mathbf{r}} - \frac{ih}{k_s^{(l)}} \hat{\boldsymbol{\phi}} \right) \right. \\
 &\quad \left. - \frac{\partial J_n(\eta_s^{(l)}r)}{\partial r} \cdot \frac{\cos(n\phi)}{\sin(n\phi)} \left(\frac{ih}{k_s^{(l)}} \hat{\mathbf{r}} + \hat{\boldsymbol{\phi}} \right) \right. \\
 &\quad \left. - \frac{(\eta_s^{(l)})^2}{k_s^{(l)}} J_n(\eta_s^{(l)}r) \frac{\cos(n\phi)}{\sin(n\phi)} \hat{\mathbf{z}} \right\}, \quad (5b)
 \end{aligned}$$

where $J_n(\bullet)$ represents the first-kind cylindrical Bessel function of order n . In the above and subsequent expressions, the superscript (1) of vector wave functions indicates that all the first-kind cylindrical Bessel functions $J_n(\bullet)$ are changed into the first-kind cylindrical Hankel functions $H_n^{(1)}(\bullet)$.

The cylindrical vector wave eigenfunctions $\mathbf{M}_{e_{on\eta_f}}(h)$ and $\mathbf{N}_{e_{on\eta_f}}(h)$ as used in (5a) and (5b) and subsequent expressions are defined as follows:

$$\mathbf{M}_{e_{on\eta_f^{(r,l)}}}(h) = \nabla \times \left[J_n(\eta_s^{(r,l)}r) \frac{\cos(n\phi)}{\sin(n\phi)} e^{ihz} \hat{\mathbf{z}} \right], \quad (6a)$$

$$\mathbf{N}_{e_{on\eta_f^{(r,l)}}}(h) = \frac{1}{\sqrt{h^2 + \eta_f^2}} \nabla \times \nabla \times \left[J_n(\eta_s^{(r,l)}r) \frac{\cos(n\phi)}{\sin(n\phi)} e^{ihz} \hat{\mathbf{z}} \right]. \quad (6b)$$

The eigenvalues, $\eta_f^{(r,l)}$, satisfy the relations of $h^2 = (k_f^{(r,l)})^2 - (\eta_f^{(r,l)})^2$, and the superscript (1) of the vector wave functions denotes the third-type cylindrical Bessel function or the first-type cylindrical Hankel

function $H_n^{(1)}(\eta_f^{(r,l)} r)$ used in the expression of the cylindrical wave vector functions for the out-going waves.

The electric type of DGF satisfies the following boundary conditions at the cylindrical interfaces $\rho = a$ and $\rho = b$ in the three-layer structure.

$$\hat{\rho} \times \overline{\mathbf{G}}_e^{(21)} = 0, \quad \text{at } \rho = a; \quad (7a)$$

$$\hat{\rho} \times \overline{\mathbf{G}}_e^{(11)} = \hat{\rho} \times \overline{\mathbf{G}}_e^{(21)}, \quad \text{at } \rho = b; \quad (7b)$$

$$\frac{1}{\mu_1} \hat{\rho} \times \left[\nabla \times \overline{\mathbf{G}}_e^{(11)} - \xi_1 \overline{\mathbf{G}}_e^{(11)} \right] = \frac{1}{\mu_2} \hat{\rho} \times \left[\nabla \times \overline{\mathbf{G}}_e^{(21)} - \xi_2 \overline{\mathbf{G}}_e^{(21)} \right],$$

at $\rho = b$; (7c)

where $\overline{\mathbf{G}}_e^{(21)}$ is given as follows:

$$\begin{aligned} \overline{\mathbf{G}}_{es}^{(21)}(\mathbf{r}, \mathbf{r}') = & \frac{i}{4\pi(k_1^{(r)} + k_1^{(l)})} \int_{-\infty}^{\infty} dh \sum_{n=0}^{\infty} (2 - \delta_n^0) \\ & \times \left\{ \mathbf{V}_{e_{o n \eta_2}^{(r)}}^{(1)}(h) \left[\mathcal{C}_1 \mathbf{V}'_{e_{o n \eta_1}^{(r)}}(-h) + \mathcal{C}_2 \mathbf{W}'_{e_{o n \eta_1}^{(l)}}(-h) \right] \right. \\ & + \mathbf{V}_{e_{o n \eta_2}^{(r)}}^{(1)}(h) \left[\mathcal{C}_3 \mathbf{V}'_{e_{o n \eta_1}^{(r)}}(-h) + \mathcal{C}_4 \mathbf{W}'_{e_{o n \eta_1}^{(l)}}(-h) \right] \\ & + \mathbf{W}_{e_{o n \eta_2}^{(l)}}^{(1)}(h) \left[\mathcal{C}_5 \mathbf{V}'_{e_{o n \eta_1}^{(r)}}(-h) + \mathcal{C}_6 \mathbf{W}'_{e_{o n \eta_1}^{(l)}}(-h) \right] \\ & + \mathbf{W}_{e_{o n \eta_2}^{(l)}}^{(1)}(h) \left[\mathcal{C}_7 \mathbf{V}'_{e_{o n \eta_1}^{(r)}}(-h) + \mathcal{C}_8 \mathbf{W}'_{e_{o n \eta_1}^{(l)}}(-h) \right] \\ & + \mathbf{V}_{e_{o n \eta_2}^{(r)}}^{(1)}(h) \left[\mathcal{C}_9 \mathbf{V}'_{e_{o n \eta_1}^{(r)}}(-h) + \mathcal{C}_{10} \mathbf{W}'_{e_{o n \eta_1}^{(l)}}(-h) \right] \\ & + \mathbf{V}_{e_{o n \eta_2}^{(r)}}^{(1)}(h) \left[\mathcal{C}_{11} \mathbf{V}'_{e_{o n \eta_1}^{(r)}}(-h) + \mathcal{C}_{12} \mathbf{W}'_{e_{o n \eta_1}^{(l)}}(-h) \right] \\ & + \mathbf{W}_{e_{o n \eta_2}^{(l)}}^{(1)}(h) \left[\mathcal{C}_{13} \mathbf{V}'_{e_{o n \eta_1}^{(r)}}(-h) + \mathcal{C}_{14} \mathbf{W}'_{e_{o n \eta_1}^{(l)}}(-h) \right] \\ & \left. + \mathbf{W}_{e_{o n \eta_2}^{(l)}}^{(1)}(h) \left[\mathcal{C}_{15} \mathbf{V}'_{e_{o n \eta_1}^{(r)}}(-h) + \mathcal{C}_{16} \mathbf{W}'_{e_{o n \eta_1}^{(l)}}(-h) \right] \right\}; \quad (8) \end{aligned}$$

while $\mathbf{G}_e^{(11)}$ is given by:

$$\begin{aligned} \overline{\mathbf{G}}_{es}^{(11)}(\mathbf{r}, \mathbf{r}') &= \frac{i}{4\pi(k_1^{(r)} + k_1^{(l)})} \int_{-\infty}^{\infty} dh \sum_{n=0}^{\infty} (2 - \delta_n^0) \\ &\times \left\{ \mathbf{V}_{e_{o n \eta_1}^{(r)}}^{(1)}(h) \left[\mathcal{D}_1 \mathbf{V}_{e_{o n \eta_1}^{(r)}}'^{(1)}(-h) + \mathcal{D}_2 \mathbf{W}_{e_{o n \eta_1}^{(l)}}'^{(1)}(-h) \right] \right. \\ &+ \mathbf{V}_{e_{o n \eta_1}^{(r)}}^{(1)}(h) \left[\mathcal{D}_3 \mathbf{V}_{e_{o n \eta_1}^{(r)}}'^{(1)}(-h) + \mathcal{D}_4 \mathbf{W}_{e_{o n \eta_1}^{(l)}}'^{(1)}(-h) \right] \\ &+ \mathbf{W}_{e_{o n \eta_1}^{(l)}}^{(1)}(h) \left[\mathcal{D}_5 \mathbf{V}_{e_{o n \eta_1}^{(r)}}'^{(1)}(-h) + \mathcal{D}_6 \mathbf{W}_{e_{o n \eta_1}^{(l)}}'^{(1)}(-h) \right] \\ &\left. + \mathbf{W}_{e_{o n \eta_1}^{(l)}}^{(1)}(h) \left[\mathcal{D}_7 \mathbf{V}_{e_{o n \eta_1}^{(r)}}'^{(1)}(-h) + \mathcal{D}_8 \mathbf{W}_{e_{o n \eta_1}^{(l)}}'^{(1)}(-h) \right] \right\}. \end{aligned} \quad (9)$$

The scattering coefficients can be determined from the boundary conditions at the interfaces between the regions. Due to their complexity, the complete expressions of these coefficients are omitted here.

2.3. Galerkin's Method of Moments Procedure

The cylindrical-rectangular microstrip antenna is shown in Fig. 1(b). The rectangular patch is positioned symmetrically with respect to ϕ and z at the interface of air and substrate. It is fed by a microstrip line parallel to the cylinder axis and connected to the center from its lower side. The feed line is inset a distance S from the edge of the patch. The feed line thus overlaps the patch surface by the inset distance S , and provides the continuity of current flow on the patch from the feed line to the patch.

2.3.1. Currents on the Feed Line

Due to the small width of the feeding line as compared to the guided wavelength, the ϕ component of the incident current may be neglected [23].

$$\mathbf{J}_z^{\text{inc}}(\phi, z) = \hat{z} \times [J_c(\phi, z) - iJ_s(\phi, z)], \quad (10a)$$

$$\mathbf{J}_z^{\text{ref}}(\phi, z) = \hat{z} \times [J_c(\phi, z) + iJ_s(\phi, z)], \quad (10b)$$

where for $L_f - \lambda/4 < z - z_0 < -\lambda/4$ and $|\phi| < \phi_f/2$

$$J_c(\phi, z) = \frac{1}{W_f} \cos k_e(z - z_0); \quad (11a)$$

and for $L_f < z - z_0 < 0$ and $|\phi| < \phi_f/2$

$$J_s(\phi, z) = \frac{1}{W_f} \sin k_e(z - z_0). \quad (11b)$$

In (11a) and (11b), $z_0 = S - L/2$ represents the z -coordinate of the feed line end (provided that the patch is centered at the origin), and L_f stands for the length of the feed line. The currents in (10a) and (10b) represent quasi-TEM incident and reflected waves on the feed line. As discussed in [23], J_z^{inc} and J_z^{ref} are expressed in terms of J_c and J_s , and truncated so that there is no discontinuity at the end of the line. The length L_f is chosen as a multiple of $\lambda/2$, to avoid nonphysical current discontinuities at the end [23].

The solution for the open-circuited line requires the propagation constant of an infinitely long microstrip line. The electrical thickness of the substrate is such assumed that only the fundamental microstrip mode propagates. A quasi-static value [24] could be used to obtain reasonably good results. The more rigorous full-wave solution was obtained and also reported in [23, 25].

2.3.2. Microstrip Patch Currents

Over the microstrip antenna patch, the currents are expanded in terms of entire-domain sinusoidal functions, in both ϕ - and z -directions [25], as follows:

for $|z| < d_0$, $|\phi| < \phi_0$, and $p = 1, 2, \dots, P$

$$J_z^{\text{patch}}(\phi, z) = \frac{1}{w_0} \sin \left[\frac{p\pi(z + d_0)}{2d_0} \right]; \quad (12a)$$

and for $|z| < d_0$, $|\phi| < \phi_0$, and $q = 1, 2, \dots, Q$

$$J_\phi^{\text{patch}}(\phi, z) = \frac{1}{2d_0} \sin \left[\frac{q\pi(\phi + \phi_0)}{2\phi_0} \right]; \quad (12b)$$

where $\phi_0 = w_0/2b$ with w_0 equal to the patch length along the ϕ -direction. To minimize complexity in the solution, the edge effect is not included.

2.3.3. Junction Overlap Currents

To provide continuity of current flow from the feed line to the patch, we introduce piecewise sinusoidal (PWS) basis functions to model the currents in the junction region. This current density is expanded

into sinusoidal functions by parts and is superimposed on the feeding stripline and microstrip antenna, as follows:

$$J_z^{\text{jun}}(\phi, z) = \sum I_m J_j(\phi, z), \quad m = 1, 2, \dots, M \quad (13a)$$

where for $|z - z_m| < l$ and $|\phi| < \phi_f$, the basis functions are defined as

$$J_j(\phi, z) = \frac{1}{w_f} \frac{\sin k(l - |z - z_m|)}{\sin kl}, \quad (13b)$$

with z_m being the center coordinate of the piecewise mode which is chosen as $z_m = -ml$ (where $m = 1, 2, 3, \dots$, and l is equal to half of the mode length). The current is assumed to be uniform across the strip width. Typically convergence is achieved fast by including three to four PWS modes. The constant k is theoretically arbitrary, but it is practically chosen as k_e for convenience.

With the expansion current modes introduced above, the integral equation, after the Galerkin's procedure in method of moments is used, is reduced to the matrix equation, which is written in a compact form as follows [25, 26]:

$$\begin{bmatrix} T_z/G_{zz}/J_r & T_z/G_{zz}/J_j & T_z/G_{zz}/P_z & T_z/G_{z\phi}/P_\phi \\ J_j/G_{zz}/J_r & J_j/G_{zz}/J_j & J_j/G_{zz}/P_z & J_j/G_{z\phi}/P_\phi \\ P_z/G_{zz}/J_r & P_z/G_{zz}/J_j & P_z/G_{zz}/P_z & P_z/G_{z\phi}/P_\phi \\ P_\phi/G_{zz}/J_r & P_\phi/G_{zz}/J_j & P_\phi/G_{zz}/P_z & P_\phi/G_{z\phi}/P_\phi \end{bmatrix} \cdot \begin{bmatrix} -R \\ I_m \\ K_p \\ L_g \end{bmatrix} = \begin{bmatrix} T_z/G_{zz}/J_i \\ J_j/G_{zz}/J_i \\ P_z/G_{zz}/J_i \\ P_\phi/G_{z\phi}/J_i \end{bmatrix} \quad (14)$$

where the following notations are implied:

- T_z , a single sinusoidal test/weighting function on the feed line,
- J_j , a series of M sinusoidal functions by parts in the junction,
- P_z , a series of P functions in the entire domain for the patch current along the z -direction,
- P_ϕ , a series of Q functions in the entire domain for the patch current along the ϕ -direction,
- J_i , the incident traveling wave current mode,
- J_r , the reflected traveling wave current mode,
- $-R$, wave amplitude of the reflected current in the line to be determined, and

- I_m , K_p , and L_q , expansion coefficients to be determined.

Obviously, there are $N = 1 + M + P + Q$ unknown coefficients. The test and weighting functions T_z are employed herein in order to enforce the number of equations to be the number of unknowns [26]. In (14), the elements of the impedance matrix represent the impedance between various test functions and expansion (basis) functions.

The expansion coefficients of the current and the reflection coefficients are obtained from the standard matrix equation, *i.e.*,

$$[\mathbf{I}] = [\mathbf{Z}]^{-1} [\mathbf{V}], \quad (15)$$

where the superscript $^{-1}$ denotes the inverse of a matrix. Once the coefficients are solved for from the linear equation system, the currents are known. Furthermore, we can calculate the far-fields and analyse the far-zone radiation patterns.

2.4. Far-Field Radiation Patterns

To obtain far-field radiation patterns of the antenna, however, calculations can be considerably simplified by using asymptotic techniques such as the steepest-descent method. Application of this method to the Sommerfeld integral in the analysis of microstrip patch antennas is presented in details in [27].

When integrating the integrand function with respect to h in the range from $-\infty$ to ∞ , we would change the cylindrical variables into spherical variables by letting

$$\eta = k \sin \beta, \quad (16a)$$

$$h = k \cos \beta, \quad (16b)$$

$$r = R \sin \theta, \quad (16c)$$

$$z = R \cos \theta; \quad (16d)$$

so that

$$\eta r + h z = k R \cos(\theta - \beta), \quad (17a)$$

$$-h \hat{r} + \eta \hat{z} = k(-\hat{r} \cos \beta + \hat{z} \sin \beta), \quad (17b)$$

$$dh = -k \sin \beta d\beta. \quad (17c)$$

As given in [8], we thus have

$$\mathbf{F}(r, z) = \int_{-\infty}^{\infty} \frac{\mathbf{G}(h)}{\sqrt{2\pi\lambda r}} e^{i(hz + \lambda r)} dh, \quad (18a)$$

$$\mathbf{F}(R, \theta) = \frac{\mathbf{G}(k \cos \theta)}{R} e^{i(kR - \pi/4)}, \quad (18b)$$

where

$$\lambda = \sqrt{k^2 - h^2}.$$

3. NUMERICAL RESULTS AND DISCUSSION

A computer program in its compact syntax form was developed using MATHEMATICA software package to compute the required dyadic Green's function components and various radiation patterns. Numerical results of antenna-radiated power patterns have been obtained in this paper for various chirality admittances. For the three-layered model, it is assumed that the relative permittivity ϵ_r of the substrate is 2.57; the radius, a , of the conducting core-cylinder is 2.5 cm; the thickness h of the chiral coating cylindrical layer is 0.012λ cm where λ is the free-space wavelength; and the cylindrical-rectangular microstrip antenna has a dimension of $2d_0 = w_0 = 4.02$ cm. The length L_f is chosen as a multiple of $\lambda_l/2$, where λ_l is the guided wavelength along the line. For the sake of comparison, the chirality admittance ξ_c is assumed to be 0, 0.001, 0.002 and 0.005, respectively.

The results of the integrals in h have been obtained by computing the integrands from $h \cong -4000$ to $h \cong 4000$. The convergence and accuracy of the problem are also considered. The summation in n was truncated at 20 because the higher-order terms are shown to be negligible. The dielectric is assumed to have a low loss, and the value of $\tan \delta = 0.001$ was introduced to shift the poles away from the real axis [25, 28].

Pozar and Voda [26] found, in the study of the rectangular microstrip antenna fed by a microstrip line on a stratified substrate, that the obtained analytical results are not too sensitive for values of $0.5 < S/(2d_0) < 0.65$ and that there is a good agreement between these results and experimental data in the case of radiating edge-fed antenna. This allows us to use a value of inset for which we can be confident that the results obtained will be reliable. We thus chose $S/(2d_0) = 0.55$ in the paper. Convergence is also tested and observed using eight sinusoidal functions in the region near the junction at $x = S - L$, for a length of $l = 0.05\lambda_e$. The feed point is centered along the radiating edge. The present method of moments solution uses three entire-domain even modes ($m = 1, 3$, and 5) along the \hat{z} -direction and three odd modes ($m = 2, 4$, and 6) along the $\hat{\phi}$ -direction, and the convergence and accuracy have been achieved.

From the obtained current distribution, we can easily get the feed line characteristic impedance. In the achiral case, the normalized resistance is a bit less than the result obtained in [26], due to the

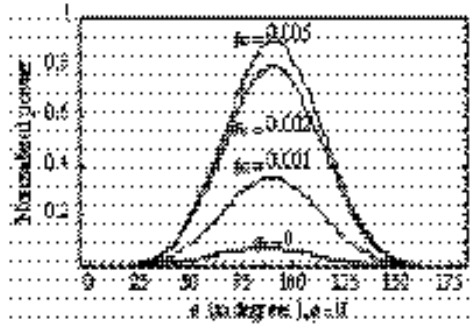


Figure 2. Normalized power versus a polar angle θ at a fixed azimuth angle $\phi = 0$ degree for different chirality admittances ξ_c .

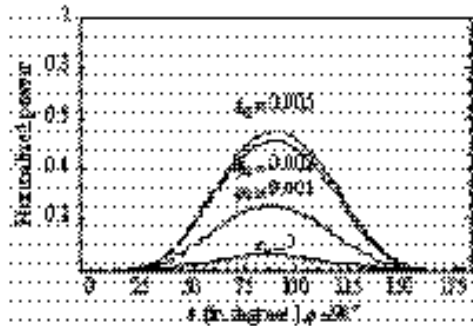


Figure 3. Normalized power versus a polar angle of θ at a fixed azimuth angle of $\phi = 90$ degrees for different chirality admittances.

effects of curvature. The resonance frequency doesn't change much with the variation of curvature, in comparison with the results in [26]. Therefore, we will not show the input impedance and resonance frequency here. Instead Figs. 2, 3, 4, and 5 show far-zone radiation patterns of the chirostrip patch under spherical coordinates, where different admittances around the resonance frequency ($f = 2.3$ GHz) are considered, respectively. The normalized radiated power patterns described by $(|E_\theta|^2 + |E_\phi|^2)/(2\eta_0)$ are plotted against the polar angle θ for different azimuth angles of ϕ . It can be seen that the features of the power pattern depend upon the chirality parameters, as shown in these figures. For given geometric sizes and dielectric parameters (such as the working frequency and the substrate thickness), the influence of the chirality admittance will change accordingly. By carefully choosing these parameters such as substrate thickness and material permittivity

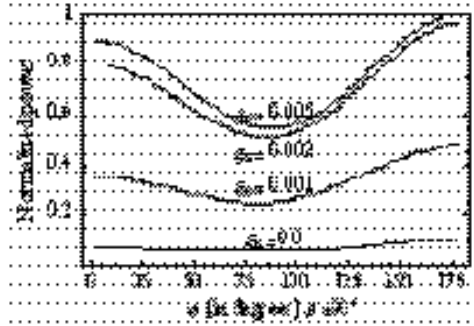


Figure 4. Normalized power versus a polar angle of ϕ at a fixed azimuth angle of $\theta = 90$ degrees for different chirality admittances.

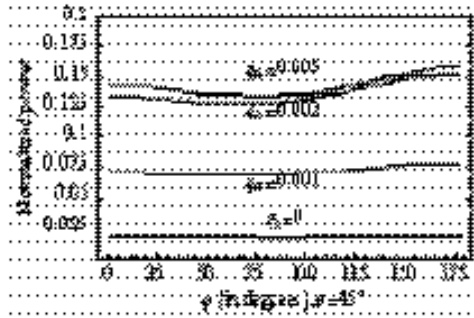


Figure 5. Normalized power versus a polar angle of ϕ at a fixed azimuth angle of $\theta = 45$ degrees for different chirality admittances.

at a given operating frequency, we can obtain the desired radiation pattern, the required 3-dB beamwidth, and minimised sidelobe levels. From these computations, it is realised that the chirality not only changes the amplitude, but also shifts the mainlobe, which is observed as well in [16, 18]. Such features can have potential applications to beam steering devices.

4. CONCLUSIONS

In this paper, radiation patterns of a three-layered cylindrical-rectangular chirostrip antenna system are investigated. The structure discussed here consists of a conducting core-cylinder, a single-layer chiral substrate coated on the core-cylinder, and a perfectly conducting and electrically thin cylindrical-rectangular microstrip patch antenna

mounted on the surface of the chiral substrate. The Galerkin's method of moments procedure and the dyadic Green's function technique are used to formulate the current distributions over the chirostrip and its feeding stripline. The dyadic Green's function in a three-layered cylindrical chiral structure is formulated and its scattering coefficients are obtained by imposing the boundary conditions on the multi-interfaces and applying the scattering superposition method. To find the far-zone fields, we obtain an asymptotic expression of DGF. This expression can be found by the method of saddle-point integration. After the Hankel functions are approximated by their asymptotic expressions, we can change the cylindrical variables into spherical variables. Then after some manipulations, the radiation patterns of such a chirostrip are obtained. A computer code is developed under MATHEMATICA software package to compute the required DGF coefficients, all the elements of the matrix in the method of moments, and the far-field radiation patterns. It is found that from the present analysis that the resonance frequency doesn't change much with the variation of curvature, but the chirality parameters and geometrical parameters can change dramatically the pattern amplitude and also shift the pattern main lobe. So, from the modelling, we can obtain the desired radiation pattern, the required 3-dB beamwidth, and minised side lobe levels.

REFERENCES

1. Krowne, C. M., "Cylindrical-rectangular microstrip antenna," *IEEE Trans. Antennas Propagat.*, Vol. AP-31, 194–199, Jan. 1983.
2. Wu, K.Y. and J. F. Kaufman, "Radiation pattern computations for cylindrical-rectangular microstrip antenna," *IEEE Trans. Antennas Propagat. Soc. Int. Symp.*, 39–42, 1983.
3. Wong, K.-L. and Y.-C. Chen, "Resonant frequency of slot-coupled cylindrical rectangular microstrip structure," *Microwave & Optical Technology Letters.*, Vol. 7, 566–570, 1994.
4. Ke, S.-Y. and K.-L. Wong, "Broadband cylindrical rectangular microstrip antennas using gap-coupled parasitic patches," *Microwave & Optical Technology Letters.*, Vol. 7, 699–701, 1994.
5. Wong, K.-L., Y.-T. Cheng, and J.-S. Row, "Analysis of a cylindrical-rectangular microstrip structure with an airgap," *IEEE Trans. Microwave Theory Tech.*, Vol. MTT-42, No. 6, 1032–1037, June 1994.
6. Chen, J.-S. and K.-L. Wong, "Mutual coupling computation of cylindrical rectangular microstrip antennas using cavity-model

- theory," *Microwave & Optical Technology Letters*, Vol. 9, 323–326, 1995.
7. Ke, S.-Y. and K.-L. Wong, "Input impedance of a probe-fed superstrate-loaded cylindrical rectangular microstrip antenna," *Microwave & Optical Technology Letters*, Vol. 7, 232–236, 1994.
 8. Tai, C. T., *Dyadic Green's Functions in Electromagnetic Theory*, 2nd edition, IEEE Press, Piscataway, New Jersey, 1994.
 9. Kong, J. A., *Electromagnetic Wave Theory*, 3rd edition, John Wiley & Sons, New York, 1990.
 10. Collin, R. E., *Antennas and Radiowave Propagation*, McGraw-Hill, New York, 1985.
 11. Chew, W. C., *Waves and Fields in Inhomogeneous Media*, Van Nostrand Reinhold, New York, 1990.
 12. Wait, J. R., *Electromagnetic Wave Theory*, Harper & Row, New York, 1985.
 13. Yin, W. and W. Wang, "Dyadic Green's function of cylindrical multilayered chiral media and its applications," *J. Electromagn. Waves Applic.*, Vol. 7, No. 7, 1005–1027, 1993.
 14. Li, L. W., P. S. Kooi, M. S. Leong, and T. S. Yeo, "Analytic representation of scattering dyadic Green's functions coefficients for cylindrically multilayered chiral media," *J. Electromagn. Waves Applic.*, Vol. 9, No. 9, 1207–1221, 1995.
 15. Engheta, N. and P. Pelet, "Reduction of surface waves in chirostrip antennas," *Electron. Lett.*, Vol. 27, 5–7, 1991.
 16. Pelet, P. and N. Engheta, "Novel rotational characteristics of radiation patterns of chirostrip dipole antennas," *Microwave Opt. Technol. Lett.*, Vol. 5, 31–34, 1992.
 17. Pelet, P. and N. Engheta, "Chirostrip antenna: Line source problem," *J. Electromagn. Waves Applic.*, Vol. 6, 771–793, 1992.
 18. Toscano, A. and L. Vegni, "Spectral dyadic Green's function formulation for planar integrated structures with a grounded chiral slab," *J. Electromagn. Waves Applic.*, Vol. 6, 751–769, 1992.
 19. Kluskens, M. S. and E. H. Newman, "Scattering by a chiral cylinder of arbitrary cross section in the presence of a half-plane," *J. Electromagn. Waves Applic.*, Vol. 6, No. 5/6, 721–731, 1992.
 20. Yi, W. and W. Wang, "Analyzing the radiated characteristics of a two-layered chirostrip dipole antenna using the dyadic Green's function," *Microwave and Optical Technology Letters*, Vol. 6, No. 4, 221–223, Mar. 1993.
 21. Zhao, H., W. Wan, and W. Yin, "Radiation characteristics of rectangular chirostrip antenna," *Tien Tzu Hsueh Pao/Acta*

- Electronica Sinica*, Vol. 25, 94–97, 1997.
22. Kong, J. A., “Theorems of bianisotropic media,” *Proc. IEEE*, Vol. 60, 1036–1046, 1972.
 23. Jackson, R. W. and D. M. Pozar, “Full-wave analysis of microstrip open-end and gap discontinuities,” *IEEE Trans. Microwave Theory Tech.*, Vol. 33, 1036–1042, 1985.
 24. Gupta, K. C., R. Garg, and I. J. Bahl, *Microstrip Lines and Slotlines*, Artech House, 1979.
 25. Silva, F. C., A. J. Giarola, S. B. A. Fonseca, and A. J. M. Soares, “Effect of a dielectric cover in a microstripline on a circular cylindrical substrate,” *IEEE Antennas Propagat. Soc. Symp. Dig.*, 508–511, 1990.
 26. Pozar, D. M., “Rigorous analysis of a microstripline fed patch antenna,” *IEEE Trans. Antennas Propagat.*, Vol. AP-35, 1343–1350, 1987.
 27. Mosig, J. R., R. C. Hall, and F. E. Gardiol, “Numerical analysis of microstrip patch antennas,” *Handbook of Microstrip Antennas*, 391–453, 1989.
 28. Collin, R. E., *Field Theory of Guided Waves*, McGraw-Hill, New York, 1960.